NSF GRANT #DMI- 0500453
NSF PRORAM NAME: Materials Processing & Manufacturing

Online Dynamic Control of Cooling in Continuous Casting of Thin Steel Slabs

Findings

In this multifaceted project to improve control of spray cooling heat transfer in continuous casting of steel with aid of fundamentally-based models, findings are presented in this report according to eight different subprojects :

1) Efficient fundamental model of solidification and temperature in thin slab casting: CON1D
2) Software Sensor, CONSENSOR
3) Online control system development, CONONLINE
4) Laboratory measurement of water flow and heat transfer during spray cooling
5) Steel plant experiments for model validation
6) Understanding defect formation during continuous casting
7) Control of mold fluid flow
8) Advance Control Algorithm Development

1. Computational model of solidification and temperature development in thin slab casting: CON1D

Primary Mold Cooling Region

A new method has been developed to accurately define the surface heat flux profile in the mold. In previous work, the CON1D model computes the surface heat flux within the mold region by solving a two-dimensional heat equation in the mold and several mass and heat balance equations within the interfacial gap[1, 2]. Its accuracy to predict mold heat transfer has been verified against a full three-dimensional finite element analysis, as well as plant measurements[3].

For the present work, the average heat flux in the mold is found from the measured temperature rise and flow rate of the cooling water, which is supplied through the level 2 system in real time. The surface heat flux profile down the mold, q_{mold} (MW/m^2), is fit with the following empirical function of time to match the average measured mold heat flux, $\overline{q}_{mold}$ (MW/m^2). This function is split into a linear portion and an exponential portion:

$$-k_{steel}\frac{\partial T_i(\pm L,t)}{\partial x} = q_{mold}(t) = \begin{cases} q_0 - q_a\cdot\left(t-t_i^0\right) & , \quad 0 \le t-t_i^0 < t_c \\ q_b\cdot\left(t-t_i^0\right)^{-n} & , \quad t_c < t-t_i^0 \le t_m \end{cases} \tag{1}$$

where t_i^0 is the start time for the slice and hence (t - t_i^0) is the time below meniscus, and n is a fitting parameter that controls the shape of the curve, chosen to be 0.4. The initial heat flux, q_0, is the maximum heat flux at the meniscus, chosen to be:

$$q_0 = \overline{q}_{mold}\cdot q_{fac} \tag{2}$$

where q_{fac} is another parameter, set to 2.3. The total time spent in the mold, t_m, is calculated by

$$t_m = \frac{z_m}{V_c} \tag{3}$$

where z_m is the mold length and V_c is the casting speed. The duration of the linear portion, t_c, is assumed to be

$$t_c = t_m\cdot t_{fac} \tag{4}$$

where t_{fac} is a third parameter, set to 0.07. Then the intermediate parameters q_a and q_b are defined below, based on keeping the curve continuous, and matching the total mold heat flux in the mold with the area beneath the curve.

$$q_a = \frac{q_0\cdot(t_c)^n(t_m)^{1-n} - (1-n)\cdot\overline{q}_{mold}\cdot t_m - n\cdot q_0\cdot t_c}{t_c^{1+n}\cdot t_m^{1-n} - \frac{1}{2}(1+n)t_c^2} \tag{5}$$

$$q_b = q_0 \cdot (t_c)^n - q_a (t_c)^{n+1} \tag{6}$$

Fig. 4 compares heat flux profiles predicted with this new model to previous measurements in thin-slab casting molds[3, 4].

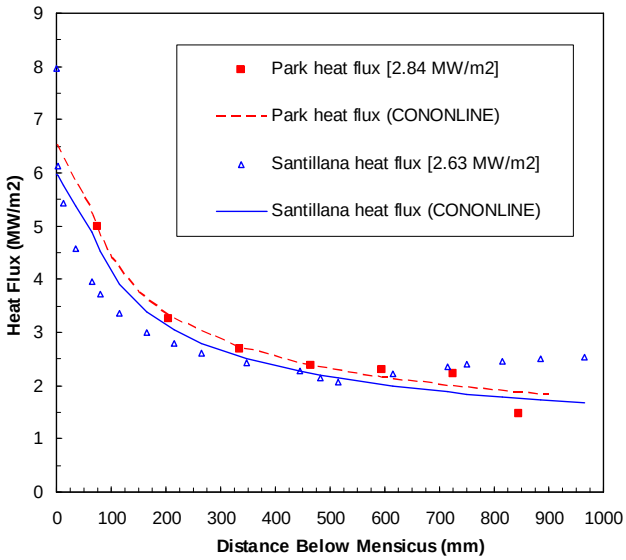

Fig. 1. Comparison of predicted mold heat flux profiles from Eqs. (2)-(7) with measurements from [3, 4]and [3, 4]

Secondary Spray Cooling Region

An example of the predicted surface temperature history from a single slice in CON1D is given in **Fig. 2**.[5] Notice that there are a number of temperature peaks and dips. The temperature dips are caused by water spray impingement and roll contact, whereas the temperature peaks occur where convection and radiation are the only mechanisms of heat extraction.

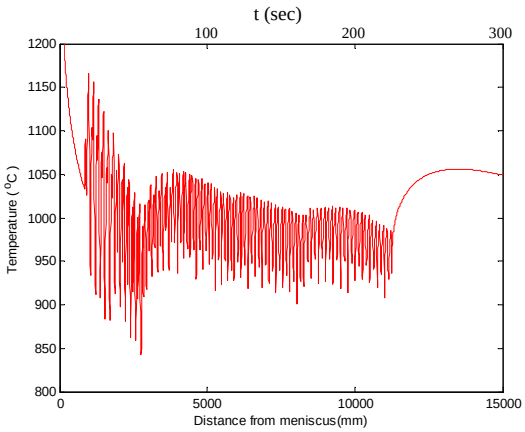

Fig. 2. Example of CON1D output: slice surface temperature history

The CON1D program has been optimized to run in less than 0.5s on a personal computer. This is necessary for it to become part of an online control system that updates every 1s. It was found that the simple explicit time-stepping method, combined with a mesh (cell) thickness of about 1mm has sufficient accuracy and stability to give optimal performance for this application. The enhancement of the heat-transfer coefficient profile to allow a more realistic (piecewise linear shape with 5 line segments) has enabled the model to readily incorporate the results from lab

experiments and to predict temperature in the plant more accurately (based on matching with experiments described in later sections).

In addition to its successful use as part of a "software sensor" (for model-based prediction and control capability), the model was used to generate setpoints for typical casting conditions. Specifically, 72 set points were generated for the typical commercial thin-slab caster at Nucor Decatur, AL to allow operation at 8 different spray-water patterns over a range of casting speeds (discretized as 9 different speeds over the maximum speed range). These set points are temperature profiles generated by CON1D using typical mold heat flux dependent on casting parameters which includes casting speed.[6, 7]

Analysis of the simulation results for different realistic setpoints (taken from the commercial caster at Nucor) revealed that the temperatures in the different zones vary slightly with casting speed, especially at low and high speed. However, a temperature-based setpoint was revealed to be a valid approach for future approach to control. This approach enables a paradigm shift for metallurgists: by focusing on optimal temperature profiles, rather than spray flow rate profiles, their activities are closer to the fundamental phenomena that control quality. Temperature is a more fundamental indicator of metallurgical embrittlement, so makes the development of spray practices for new grades and processes much easier.

The CON1D model is now a powerful tool that has been implemented as a software sensor, CONSENSOR into the control system, CONONLINE, discussed next.

2. Software Sensor CONSENSOR

The purpose of the software sensor is to provide a real-time estimate of the two-dimensional temperature distribution through the thickness and down the length of the entire strand, including the mold, spray-cooling, and radiation cooling zones.[8, 9] Attention is focused on the outer surface temperature profile, which is the most sensitive to changes during operation. This is the same function temperature sensors would perform in a traditional feedback control system. This shell surface temperature history is denoted $T(z,t)$, where z is the distance from the meniscus and t is the time.

The output domain of CON1D on a *t*-*z* plot is shown in **Fig. 3**. For constant casting speed, this domain is a line with slope $\tan(\theta)$. As the figure illustrates, at time t_0, CON1D only gives data for point z_0. In order to obtain the full temperature profile at time t_0, the results of multiple CON1D runs must be interpolated.

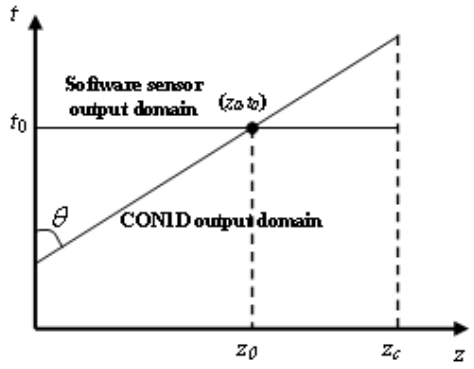

Fig. 3. CON1D and sensor output domain comparison

Keeping track of many slices through the moving shell requires increases computational time by a factor equal to the number of slices. However, it is not necessary to perform a complete run of every slice at each time step. Instead, each slice is simulated incrementally for the duration of each time step, which requires the same time as one complete simulation through the caster, ~0.6s. This is possible because conductive heat transfer is negligible in the

casting direction, as discussed in the previous section. The shell surface temperature is then approximated by interpolating the latest temperature history of each slice. This process is illustrated in **Fig. 4**.

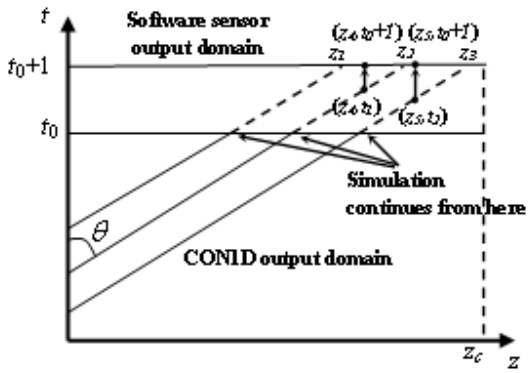

Fig. 4. Illustration of the incremental run of CON1D and shell surface temperature profile approximation

At time t_0, each of the slices is simulated for 1 second, until time $t_0 + 1$. For a caster of length 15 m operating at a casting speed of 3 m/min (50 mm/s), then 15000 / 50 = 300 slices are needed to continuously simulate the entire caster. In practice, 200 slices are used regardless of casting speed, in order to maintain a real time simulation.

At startup, CONONLINE creates new slices equally spaced throughout the caster. With 200 slices, in a 15 m long caster, there should be 75 mm between slices. Once the i^{th} slice is 75 mm from the meniscus, CONONLINE starts the $i+1^{th}$ slice. During operation, a new slice is started every time an old slice reaches the end of the caster, keeping the total number of slices constant.

Fig. 4 shows three consecutive slices. The slices are all started at different times, giving shell temperatures for different curves in the *t*-*z* domain. Then at time $t_0 + 1$, exact data is known for points z_1, z_2, and z_3. For $z_1 < z < z_2$ and $z_2 < z < z_3$, an interpolation scheme must be used. As shown in **Fig. 5**, a linear interpolation scheme between the exact data points would miss a great deal of the data in the peaks and valleys, with temperature errors possibly of 100 or more. Instead, a delay interpolation scheme is used.

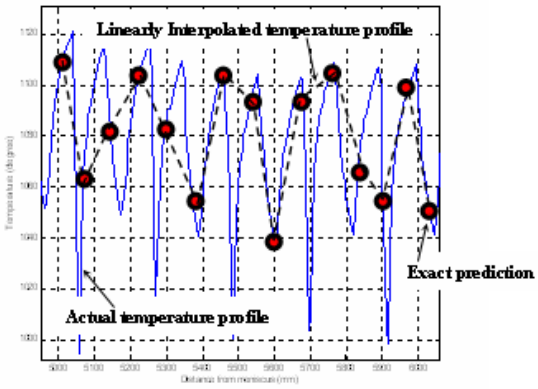

Fig. 5. Example of the actual temperature profile, the exact estimation/prediction and linearly interpolated temperature profile

This is done by using the history of the CON1D slice. $T(z_4, t_0 + 1)$ in Fig. is approximated by $T(z_4, t_2)$ from the temperature history of the middle slice. Similarly, $T(z_5, t_0 + 1)$ is approximated by $T(z_5, t_3)$ from the temperature history of the right slice. In general,

$$T(z,t) = T_{1D}^{i}(z) \text{ if } z_{i+1}(t) < z \le z_i(t)$$

where T_{1D}^{i} is the CON1D temperature history of the i[th] slice and $z_i(t)$, $z_{i+1}(t)$ are the locations of the i[th] and i+1[th] slices at time t.

The approximation error under this interpolation scheme depends on the slice spacing. The average error can be estimated as the temperature change in half the time needed for a slice to travel the distance of slice-spacing. For 75 mm-spaced slices moving at 50 mm/s, this would be 0.75 s. The temperature change in this time is typically around 30 C, and goes to zero as the system goes to steady state. The present scheme is better than linear interpolation, which still has error at steady state.

The software sensor, CONONLINE, manages the multiple slices and their respective temperature histories, and interpolates between them. It uses CON1D as a subroutine to compute each slice. CONONLINE provides an estimate of the full temperature profile in the strand to use in control calculation, including the surface temperature distribution down the strand and the location of the solidification front, (shell thickness) and metallurgical length of the liquid core inside the strand. More detail is given elsewhere.[9]

3. Online Control System Development: CONONLINE

A control system has been developed that integrates with the Level 2 system of a continuous caster, to control the spray cooling water flow rates in real time.[8, 9] The software implementation of this system includes 1) the software sensor CONSENSOR, 2) a monitor to display the results in real time, and 3) a control algorithm CONCONTROLLER to regulate the surface temperature, in addition to network software to maintain communications and shared memory. The control system is described in **Fig. 6** below. An important feature of this system is that CONSENSOR performs closed-loop estimation in the mold, and open-loop estimation in the secondary cooling (spray) zones. Loop closure at mold exit (beginning of secondary cooling) is attained by matching the total heat removal in the mold with the measured temperature rise of the mold cooling water. As described in more detail elsewhere,[10] this makes CONSENSOR a *hybrid* strand temperature observer. At present, fully closed-loop control is not possible due to the unreliability of temperature sensing in the secondary cooling region. Even with reliable pyrometers, open-loop model-based estimation still would likely be needed to fill the gaps between their highly-localized readings in order to attain reasonable control performance.

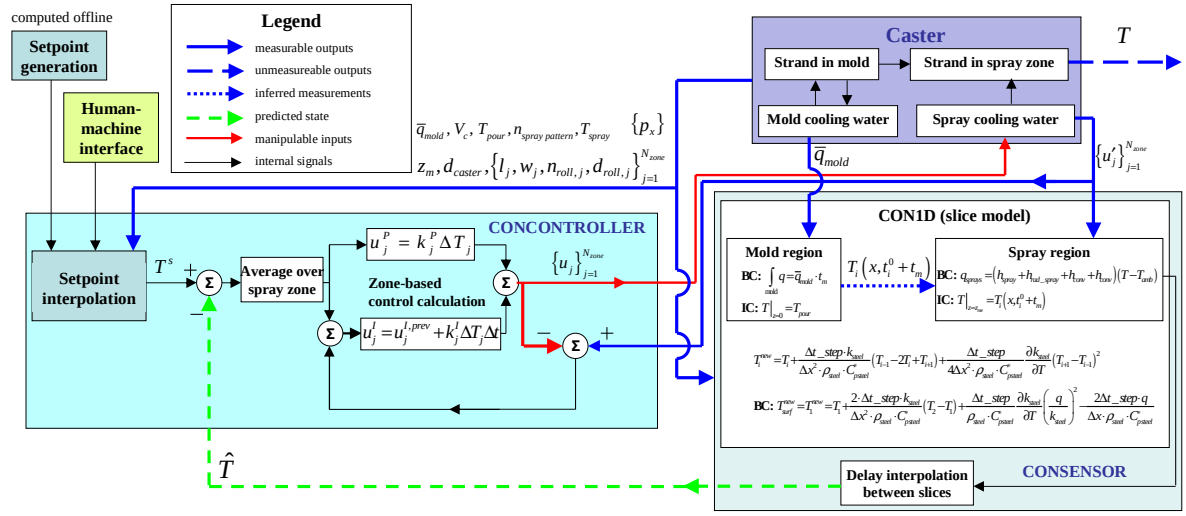

Fig. 6. Control diagram with CONSENSOR estimator/predictor and CONCONTROLLER control algorithm

CONCONTROLLER currently runs on a separate computer from CONONLINE, to ensure real-time output of spray commands even if the model runs slowly or crashes. The monitor runs on the model workstation, and takes advantage of GTK+ and GDK graphical user interface libraries. The two computers communicate with each other and the caster Level 2 system as shown in **Fig. 7**.

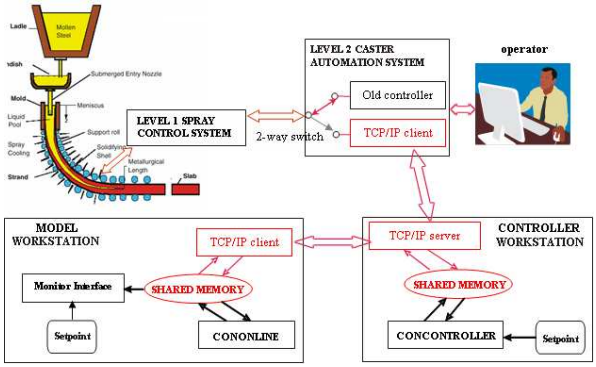

Fig. 7. Software sensor based control system architecture

Fig. 8 shows a typical snapshot of the monitor. It was developed to provide clear and quick feedback to the plant operators and engineers. The data shown includes shell surface temperature, temperature setpoint, shell profile, metallurgical length, spray water flow commands, and casting conditions. This allows for monitoring of the control system performance, warning of dangerous operating conditions, and providing general information about the current state of the steel slab.

The accuracy of control is limited first by the actual casting equipment. A continuous caster is divided into spray zones, each zone having a single water flow input. This water flow rate is the actuator controlled by CONCONTROLLER. Although there is usually more than one spray zone across the width of the caster, the output of the software sensor is only for the centerline of the slab. The spray zones outside of the center of the caster require additional logic. Currently, they are fixed fractions of the central zone, simulated by the model.

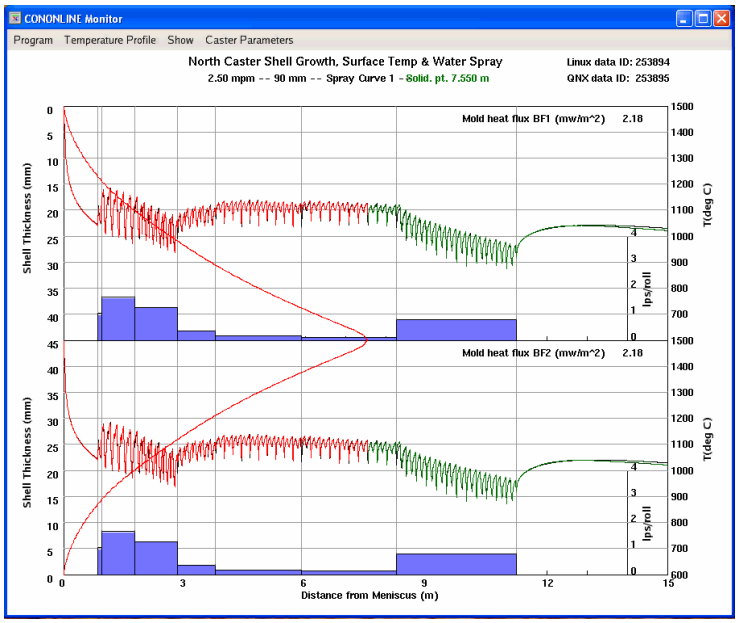

Fig. 8. Snapshot of monitor interface displaying on both sides: the shell surface temperature profile, its corresponding setpoints, the spray-water flow rates commanded and their setpoints, the shell thickness profile prediction, and other information.

Fig. 9 shows the center spray zones of the caster at the Nucor Decatur steel mill. In the first four spray zones, inner and outer radius sprays are linked. In the remaining three zones, the inner and outer radius sprays may be separately assigned. Thus, a total of 10 independent spray commands are available.

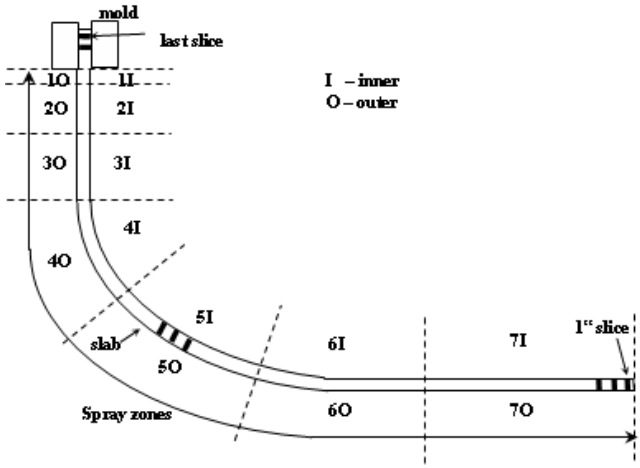

Fig.9. Center spray area configuration

Surface temperature response from conduction is faster than heat transported by the moving strand along the length of the caster, so the control of each spray zone may be governed by an independent control algorithm. Currently, these are single-input-single-output controllers. The possibility of using multiple-input-single-output or distributed-input controllers is a topic of continuing research.

Each controller follows the same general control algorithm. At each time step, the error between the shell surface temperature profile estimated by the software sensor and a setpoint temperature profile is averaged over the portion of the slab governed by the controller. This average temperature error is used to calculate control effort based on a proportional-integral control law. The gains are tuned separately for each spray command.

The actual spray command is limited to a range between turning closing the control valves and opening them completely, and so the effect of actuator saturation is a concern. Integrator windup can lead to over or undershooting should saturation occur during transient behavior. A classical anti-windup scheme [11] is applied to prevent integrator windup if the control command becomes negative or greater than the maximum possible spray rate. More detail on the controller design is given elsewhere.[9]

Choosing temperature setpoints is a challenging task that is on-going. Initial setpoints have been based on sets of water flow-rate setpoints that yield good performance in the steady state from past experience. A complete set of spray rates for all spray zones at all casting speeds is called a spray pattern. Each spray pattern is typically tuned for a specific grade of steel. It is designed to achieve a surface temperature history that avoids cracks, while solidifying the steel prior to exit from the containment region.

Fig. 10 and **Fig. 12** show results of offline testing using the control system. These figures show the outputs of the software sensor under different control strategies in order to illustrate some of the issues involved in implementing software sensor-based control. Running in real time, they include the same numerical errors encountered in the caster. In partnership with Nucor Steel Decatur, the model is being tested on an actual caster in “shadow mode”, prior to implementing the control system commercially.

Fig. 10 compares the performance of the online control system to the current spray practices during a rise in casting speed from 2 to 2.5 m/min. The shell surface temperature at 11.2 m below the meniscus, the end of containment in the simulated caster, is plotted. The conventional control scheme is based on interpolation between fixed water-flow setpoints.

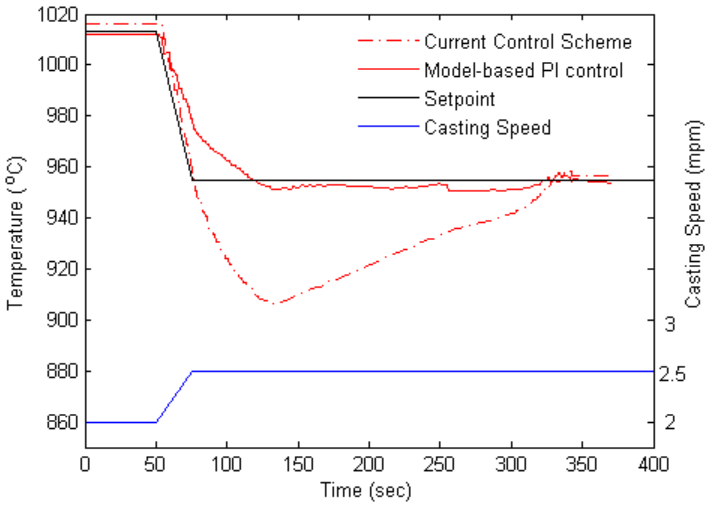

Fig. 10. Surface temperature histories predicted at 11200mm below meniscus for conventional and new model-based control systems, showing that new controller better tracks surface temperature during a change in casting speed

During transient operation, the water flow setpoints from a spray pattern are linearly interpolated by casting speed to determine the water flow rates used. Without regard to the actual dynamics of the casting process, the current conventional control scheme increases the water flow rates proportionally to the casting speed during casting speed rises, causing overcooling of the casting slab. In **Fig. 10**, the temperature undershoot caused by this issue can be seen. These problems associated with a conventional control scheme are addressed by the model-based PI control algorithm in CONCONTROLLER, which exploits the shell temperature profile estimated by CONONLINE (and CON1D). In this case, the controller attempts to match the temperature setpoint profiles that correspond to the steady-state water flow rate setpoints.

With the software sensor based control, it is also possible to use constant temperature setpoints. This can be thought of as changing the control objective to a disturbance rejection problem, maintaining the shell surface temperature at a given profile during transient changes in casting conditions. Instead of a different temperature profile for each casting speed, a single temperature profile is chosen for the setpoints. This retains the experience and knowledge in the current spray practices, while taking advantage of the opportunities added by the software sensor.

Another problem arises, regarding heat transfer in the mold. When calculating a temperature setpoint using CON1D, an estimated mold heat removal rate and pour temperature are used. If the actual running conditions differ, the setpoint temperature at mold exit may be higher or lower than the actual temperature at mold exit. PI control, in this case, would try to eliminate this “error,” causing sharp transients in the spray zones just below the mold. However, the resulting fluctuations are more likely to cause cracking problems than the higher or lower temperature itself. To avoid these detrimental fluctuations, five different mold heat removal rates are used to create five different shell temperature setpoints. This is shown in **Fig. 11**.

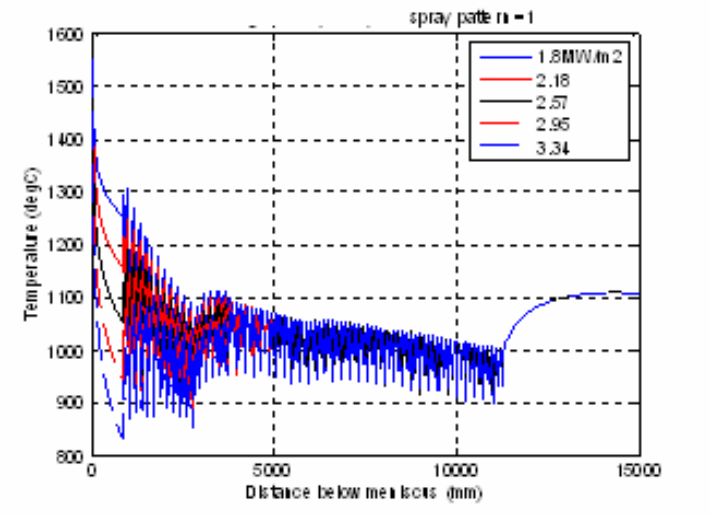

Fig. 11. The 5 temperature setpoint curves for spray pattern 1

Note that the effect of mold heat removal variations diminishes down the strand. The setpoint only needs to be adjusted in the spray zones higher up in the caster. Currently, the setpoint in the first four segments is interpolated linearly by the mold exit temperature. In the last three segments, the nominal setpoint is used.

The following results show the software sensor outputs for three different control methodologies. In all cases, the casting speed drops suddenly from 3.5 m/min to 3.0 m/min at time t=0. In **Fig. 12**-A, no control is used, and so the water spray rates remain constant. Due to the lower casting speed, the resulting surface temperatures are lower. In **Fig. 12**-B, the current spray practice is followed. When the casting speed changes, the spray rates are immediately changed according to the predetermined spray pattern. In **Fig. 12**-C, the current CONONLINE-CONCONTROLLER online control system is used to set the water spray rates.

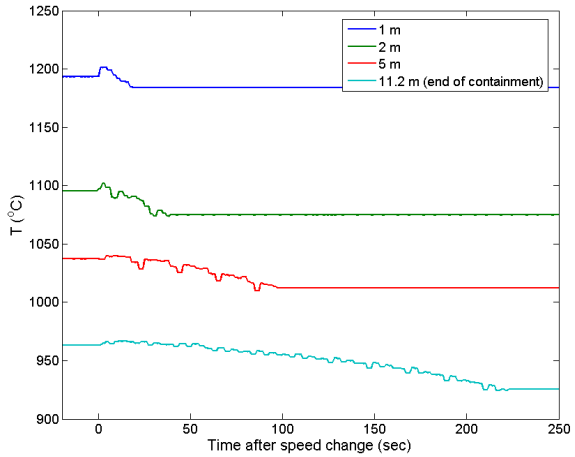

A) No spray control (constant flow rates).

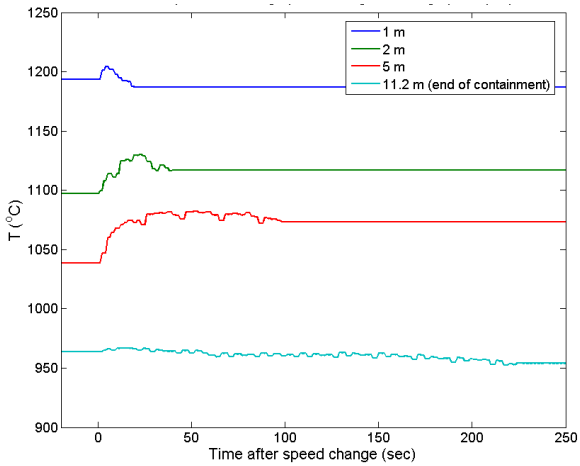

B) Conventional control (flow rates proportional to casting speed).

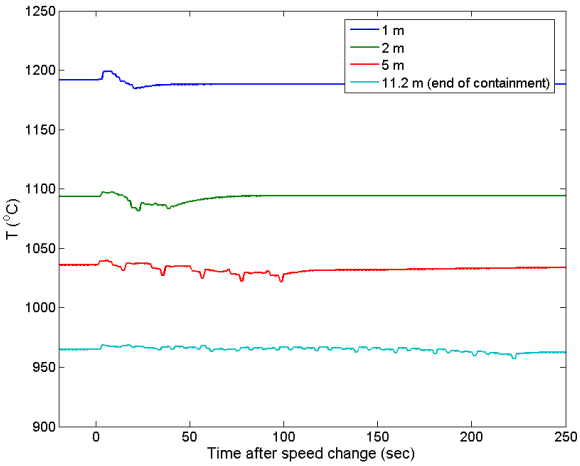

C) Software-sensor based PI control
(constant temperature setpoints)

Fig. 12. Outer shell surface temperature at different distances from meniscus after casting speed drop.

A few effects are observed in all three cases. There is a rise in temperature immediately after the casting speed changes due to the decrease in mold heat removal rate that accompanies the speed drop. This increase, as described above, decreases in magnitude lower down the caster. A small amount of periodic error can be seen in all three graphs. This is due to the delay interpolation described previously. Finally, steady state is not reached until the steel at every point in the caster has been cast entirely at the new conditions. The transient period therefore increases with longer distances from the meniscus.

If no control is used, the surface temperature drops throughout the caster due to the lower casting speed as shown in **Fig. 12**-A. Transient behavior with overshoots is produced by conventional control (**Fig. 12**-B). Note that the steady state change in temperature differs throughout the caster. At some distances, the final temperature is lower after the speed change while at others it is higher. This system does not account fo the dynamics of the moving steel strand. The new software-sensor based control system avoids these problems, as the spray rates are changed sequentially to roughly achieve the desired steady state performance (**Fig. 12**-C).

This new software-sensor based control system will improve steel quality at the steel plant, by maintaining temperature in the process more closely during transients. A complete description of the system is given elsewhere.[8, 10] An advantage of CONONLINE, beyond its use for control, is that it offers more information to plant engineers and operators regarding the effect that casting conditions have on the strand. Moreover, the system, which

runs in real time and accurately represents the behavior of a real caster, is a valuable research tool that enables scientific investigation of the continuous casting process. Future advances in control strategies and quality understanding can now be investigated using this system.

4. Laboratory measurement of water flow and heat transfer during spray cooling:

Fundamental experiments will give a better understanding of water spray cooling at high temperatures using water jet / air mist or "pneumatic" cooling nozzles. Specifically, the heat transfer coefficients that characterize heat removal from the hot steel surface have been extracted from the measurements. Heat removal depends on the water condition at the interface, which involves film boiling and the Leidenfrost effect. When two layers form: water above a thin layer of steam, then the heat transfer is relatively steady. However, spray heat transfer is often dynamic and is a complex function of droplet momentum, surface roughness, and surface temperature. Pneumatic nozzles may increase the Leidenfrost temperature to such a high value that heat transfer is always in the transient boiling regime. Thus, further research is needed not just on measuring the heat flux during spray cooling, but also on understanding the nozzle characteristics which control this behavior. The collaboration with Cinvestav aims to investigate these issues, using both transient and steady-state experiments.

In **Fig. 13**, typical results from the water impact density distribution laboratory experiments are shown for a nozzle at both maximum and minimum operating conditions.

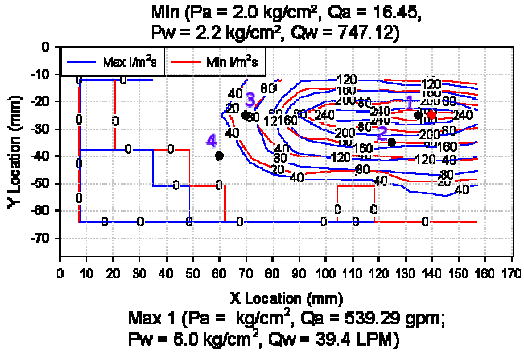

Fig. 13. Spray pattern corresponding to minimum and maximum operating conditions. Black dots thermocouple locations and the red dot is the nozzle centerline.

In this project, the spray patterns of all the Delavan Spray Technology nozzles used in the Nucor Decatur and Riverdale casters were measured. The water spray rate maps give the shape of the water droplet impact distribution over the height of the pattern and are needed for developing a fundamental-based model of heat transfer convection rates. This measurement also provides a simple method to maintain uniform heat transfer by showing how to position nozzles to cover the whole area it is designed to cool. During this research, it was found that two of the nozzles were not, in fact, covering the whole width of the area that they were supposed to cool as shown in **Fig. 14**.

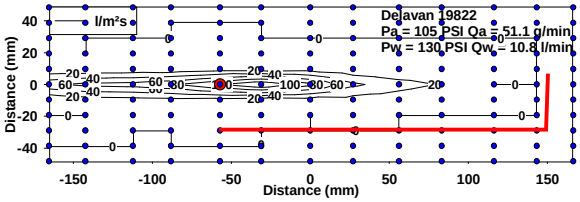

Fig. 14. Measured spray pattern and corresponding width from the caster blueprints marked a red line. Blue dots collector locations and the red dot is the nozzle centerline.

A typical example of the cooling curves measured with the transient heat transfer measurement apparatus at Cinvestav is shown in **Fig. 15**.

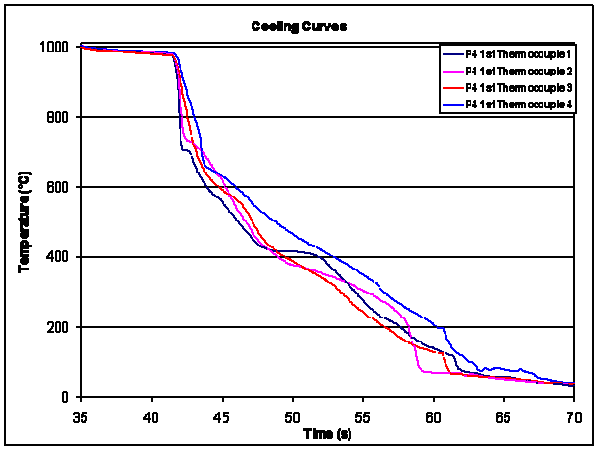

Fig. 15. Cooling curves from a transient experiment

Heat flux and temperature on the surface of a sample is determined using a computer program CONTA developed in Michigan State University and Sandia National Laboratories. The program solves nonlinear, one-dimensional planar inverse heat conduction problem (IHCP) using finite difference method (FDM) based on implicit Crank-Nicolson method. When measuring large cooling rates, the calculated heat flux has errors, as they do not reproduce the measured temperatures when used as the boundary condition of a direct heat transfer solver. To overcome this problem, the original data was augmented by linear interpolating new data between the measured data points. The correlation obtained can be seen from **Fig. 16**.

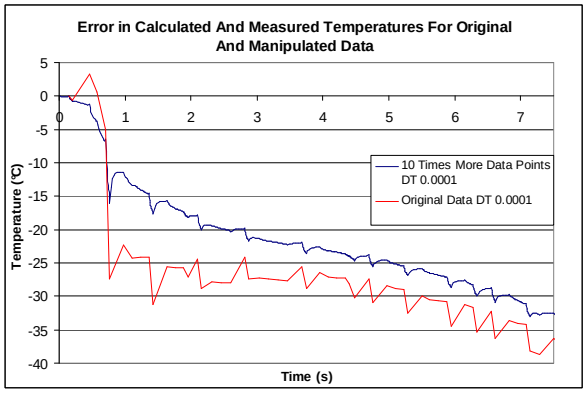

Fig. 16. Heat flux values from centre of a water spray nozzle impact pattern as a function calculated surface temperature.

During each experiment, the sample is heated in stages from 100 ^{o}C to 1300 ^{o}C in steps of 100 ^{o}C, as shown in **Fig. 17**. At each step, sample temperature is held for 7 minutes, while temperatures in the sample and ceramic body and the power input are all recorded. This method enables measurement of the transient heat extraction changes that occur during spraying at a constant temperature independently from the changes due to changing temperature.

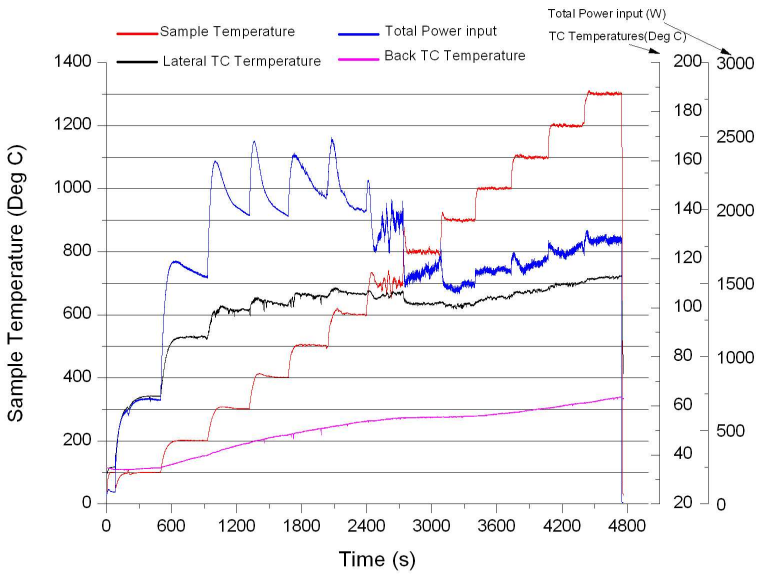

Fig. 17. Sample heating up path with lateral thermocouple temperature, back thermocouple temperature and total input power.

To interpret the experimental measurements (ie. extract the spray heat transfer coefficients), a two-dimensional axisymmetric transient heat-conduction model has been constructed using the commercial FEM-based software package COMSOL (www.comsol.com). The domain, shown in **Fig. 18** includes the sample, the copper coil, and the ceramic body. Each simulation begins by solving for the quasi-static vector magnetic potential field and the resulting heat generation from both the induced and applied currents is input as a source term to the heat transfer calculation. Since the copper induction coil consists of 1.5 loops, both 2-D axisymmetric geometries are created of both both 1-loop and 2-loop geometries and the final predictions are generated by combining results appropriately from simulations of both geometries.

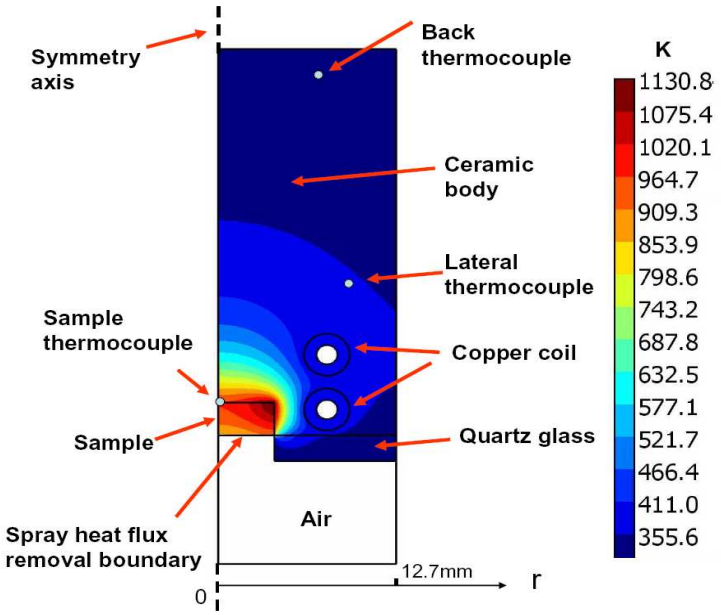

Fig. 18. Model domain for 2-loop geometry with temperature contours (600^{o}C sample temperature).

Typical results from the new steady state measurement system are shown together with results from transient measurements in **Fig. 19**.

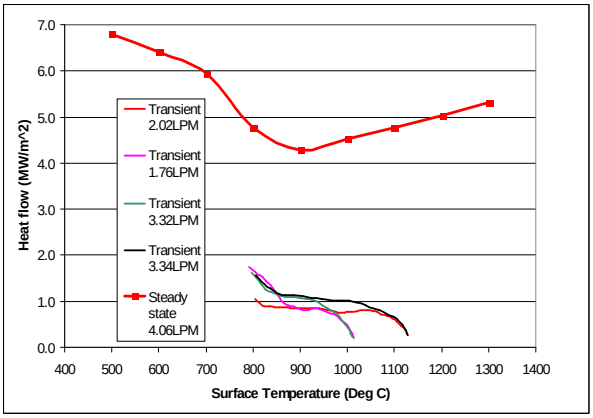

Fig. 19. Heat flux at centre of a water spray nozzle impact pattern as a function calculated surface temperature.

It is difficult to draw firm conclusions from this experiment, owing to the difficulties in avoiding sample oxidation, measuring thermal efficiencies, extracting accurate temperatures and obtaining repeatable results. However, these preliminary results show that these measurements can be made and the preliminary results in **Fig. 19** suggest that the transient experiment produces much lower heat transfer coefficients than the steady state experiment. This might be due to the time needed to establish the boundary layers, or due to thermocouple delays. The initial portion of each transient experiment is similar. After several seconds, the transient measurements start to approach the steady-state predictions, as indicated by the similarity between the heat fluxes at 700°C and lower.

Future improvements, change material from steel to platinum, cooling water temperature measurements, new DAQ-system, better insulation of the sample from moisture on other surfaces except the front, and direct measurement of the operating current, are planned to improve the ability to measure heat extraction. Also calculation of the surface temperature will be improved by using a more advanced heat transfer model, such as 3-D. More details on this work are given elsewhere.[5, 12, 13]

5. Steel Plant Experiments for Model Validation and Calibration

Sample data measured at the caster is shown in **Fig. 20** for the case of changing spray pattern at constant casting speed change at north caster (01/13/06 9.52 am – 10.04 am, south caster 01/13/06 16.12 – 16.37);

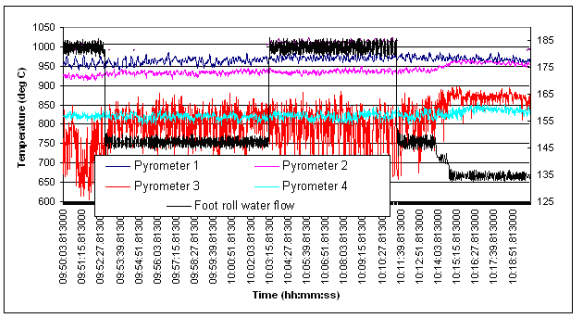

Fig. 20 Pyrometer Data during spray water change trial 1 (3.5 m/min; spray pattern 4)

The pyrometer measurements varied throughout the experiments, due to the intermittent presence of steam, and possibly also due to variations in emissivity of the surface scale layer. For the sample raw data given in **Fig. 20**, (trial 1), pyrometers 1,2 and 4 are seen to have relatively uniform temperatures while pyrometer 3 fluctuates over several hundred degrees. Blowing the steam away with a fan was found to increase and stabilize the pyrometer temperatures, producing the mean values included as part of **Fig. 21**.

To compare with the pyrometer measurements, the varying surface temperatures computed by the CON1D model are averaged over 20mm of strand surface within the varying jet impingement region, which corresponds to the region that the pyrometer measures (in between rolls). This mean temperature is compared with the 4 pyrometer measurements in **Fig. 21**, along with the entire temperature profile. The agreement is reasonable, although further calibration is needed. **Fig. 21** also reveals the variations in the surface temperature, which need further work to validate.

The results from this run show that the entire processing time for this 90-mm thick strand from liquid to complete solidification takes only 1-3 minutes. Casting speed variations from 3-5m/min result in metallurgical lengths ranging from 6-13m for these typical thin slab casters. The metallurgical length for the 3.5m/min case shown is ~11m.

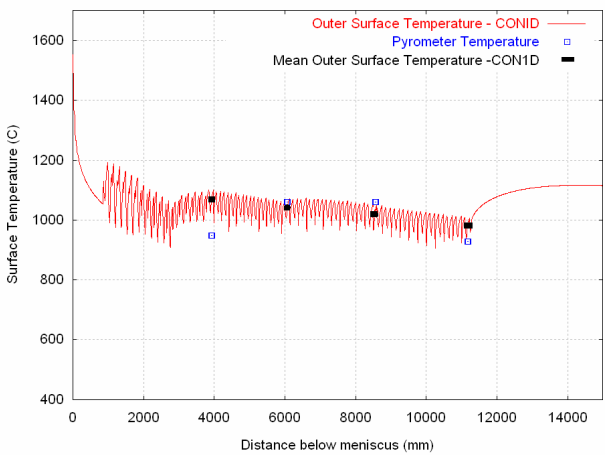

Fig. 21 Surface temperature history at steady state, comparing CON1D model predictions and steel plant measurements (3.5 m/min; spray pattern 4)

In further calibration of the model to match pyrometer measurements outside of the caster, (which is the most reliable), and to match the formation of whale defects, it was discovered that the pyrometers in the spray zones must have been measuring lower values than the actual temperatures, for reasons discussed previously. Thus, the surface temperature predicted by the model exceeds those pyrometer measurements for the better calibration, as shown in **Fig. 22**.

Although model validation is ongoing, the CON1D model was found to be sufficiently accurate to implement into the control model, owing to its ability to correctly predict the formation of a whale in the South Caster, and the avoidance of whales for other conditions.

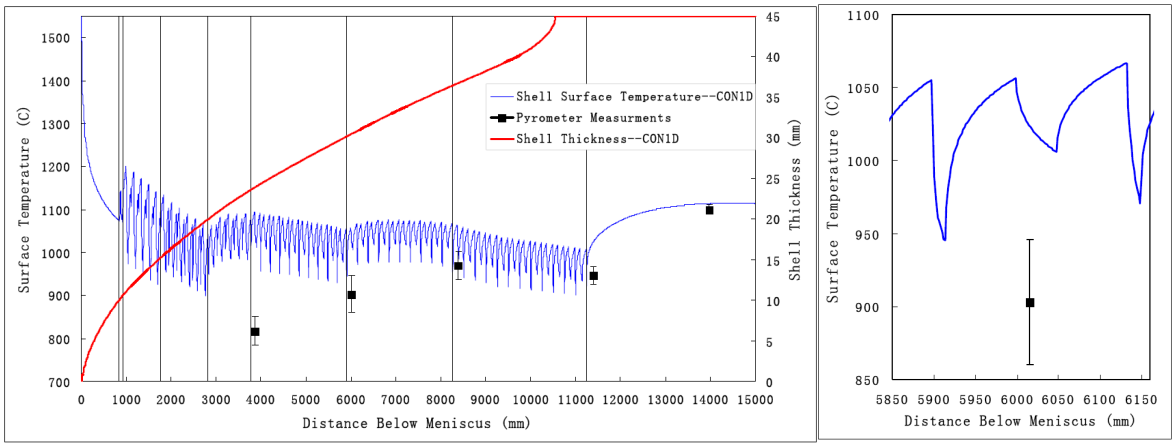

a) along entire domain b) close-up near one roll spacing

Fig.22. Shell surface temperature comparison of CON1D predictions and pyrometer measurements

At Mittal Riverdale, surface temperature is measured for different casting speed and spray water flow rates using four pyrometers: including one at the bend, (10256mm below the meniscus, one at the shear, (14550mm below meniscus), and two in the spray zones. So far, three trials (trial 1 on Sep.11th, trial 2 on Oct.19th and trial 3 on Mar.12th) have been conducted at steady conditions. Simulations of six cases (case 1~6, two for each trial) have been performed to predict the strand surface temperature, which are then compared with the pyrometer measurements.

The pyrometer measurements fluctuated throughout the trials, due to the intermittent presence of steam, possible variations in emissivity of the surface scale layer, and changes in casting conditions. Time periods of steady casting, with relatively uniform pyrometer temperatures, were chosen to get average measured temperatures.

Fig. 23 and **Fig. 24** and show typical spray-zone pyrometer measurements for case 5 in trial 3. These pyrometers were put in the same location of segment 2, 5361mm below meniscus. Pyrometer measurements varied by 20°C between different two-color methods and 200°C over 90 minutes time intervals of roughly steady casting. The ~40-minute time period over which the measured temperature is averaged, is also shown in the figures.

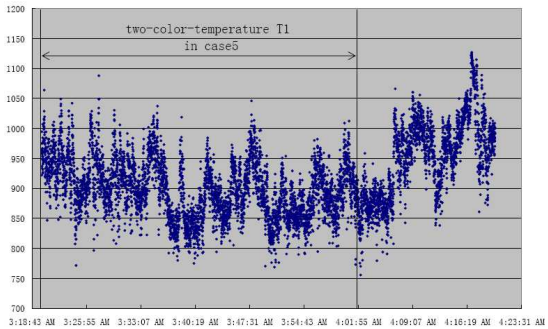

Fig. 23. Two-color-temperature T1 in case 5

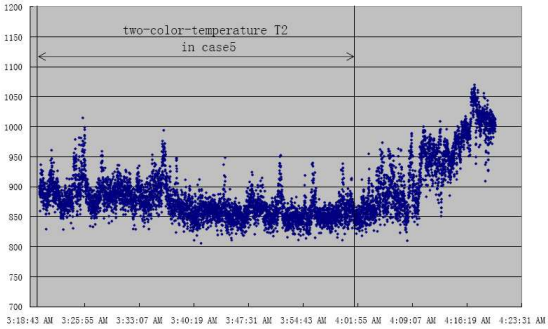

Fig. 24. Two-color-temperature T2 in case 5

Fig. 25 and **Fig. 26** show simulation results for case 5. Measurements from the pyrometers are included for comparison The model temperature predictions are mainly within the scatter of the measurements, so are considered to be reasonable. This degree of agreement was also found for most casting conditions in other cases, especially within the spray zones.

The results from this run show that the entire processing time for this 55-mm thick strand from liquid to complete solidification takes only 1-2 minutes. A casting speed of 4.5m/min results in a metallurgical length of 4.6m for this typical thin slab caster.

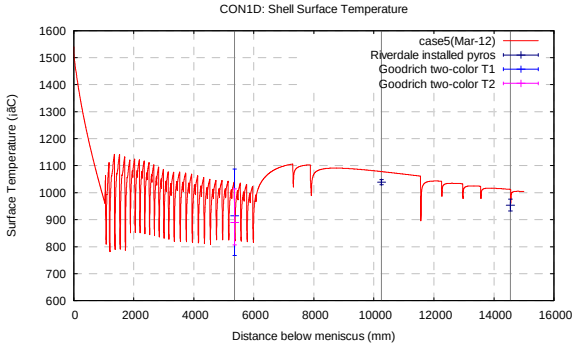

Fig. 25. Temperature prediction and comparison

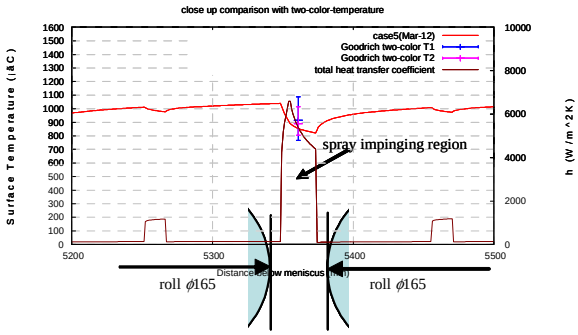

Fig. 26. Close up comparison with two-color-temperature

Validation and improvement of the CON1D model is still ongoing. Quantitative accuracy of the model is essential to avoid defects, such as whale formation. In the meantime, the model has been implemented into the CONONLINE control model system and is being tested in the plant, where quantitative accuracy is not essential to improve over the existing control model.

6. Understanding Defect formation during Continuous Casting:

New insight into the mechanism of formation of defects associated with secondary spray cooling is being obtained. These surface defects often initiate in the mold[14], especially at the meniscus[15], and later form surface cracks far below the mold in the secondary spray cooling zones. Cracks form at the roots of oscillation marks, which are prone to transverse crack formation during the spray cooling, depending on the temperature history, and the formation of embrittling precipitates. Thus, oscillation mark depth, hook formation, and other defects are also being studied. To avoid cracks, it is often necessary to keep the strand above a certain critical temperature, such as the Ar_3 temperature, ~700°C.[16]

The model to predict precipitate formation, is described in detail elsewhere.[17] It features a new, efficient algorithm to simulate size distributions, starting with an equilibrium model (to predict supersaturation), and coupled with a size-group model, with time-efficient implicit method to predict particle particle nucleation and growth from single molecules to full-size particles, based on diffusion and curvature-based surface tension considerations. In preliminary results, the model has been applied onssuccessfully to predict the size distribution of Al-N precipitate particles measured in a typical continuous cast steel slab. **Fig. 27** shows validation of the model with analytical solution, and **Fig. 28** shows the comparison with the measured distribution.

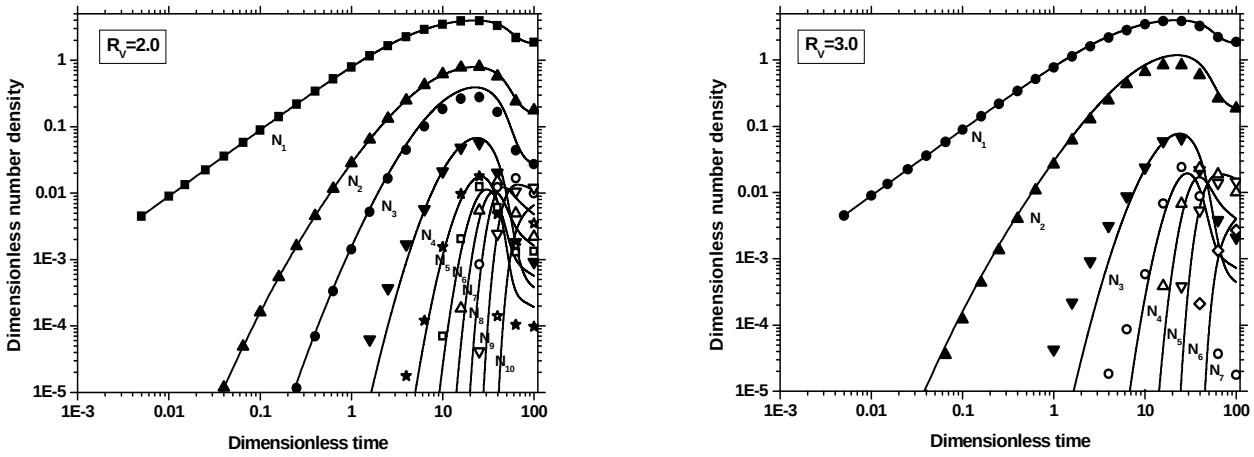

Fig. 27. Diffusion results of each size group by PSG method compared with exact solution for different R_V

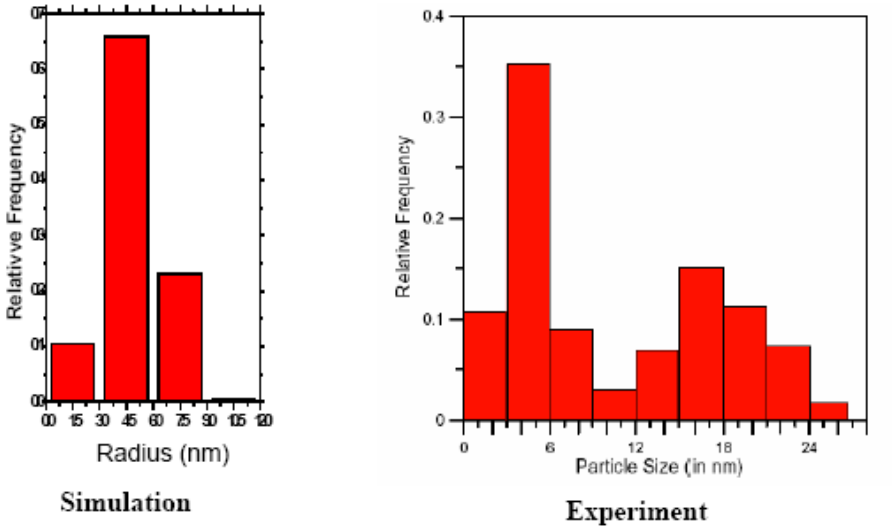

Fig. 28. Comparison of AlN size distribution between PSG method and measurement[17]

7. Control of Mold Fluid Flow:

The 3-D computational model was validated by comparing results with an analytical solution and with nail board and oscillation mark measurements collected at the plant (see **Fig. 29**). Increasing EMBr strength at a constant SEN depth is found to cause a deeper jet impingement, weaker upper recirculation zone and meniscus velocity, and a smaller meniscus wave. Increasing SEN depth without EMBr caused the same trends. Increasing SEN depth at a constant EMBr strength brought about the opposite: higher meniscus velocity, larger meniscus wave, and deeper penetration depth. Using the knowledge gained from this model, electromagnetic forces can be controlled to stabilize the fluid flow in the mold cavity and thereby minimize casting defects. Further details are found elsewhere.[18]

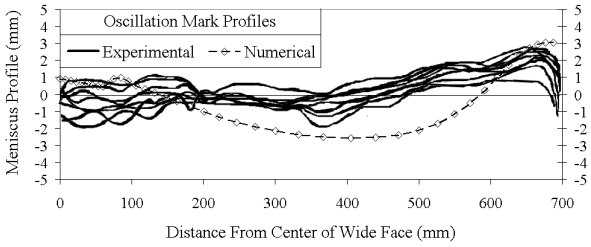

Fig. 29. Comparison of calculated meniscus profile from Case 6 with oscillation marks

8. Advanced Control Algorithm Development:

Research in online control algorithms lays the foundation for improved optimal prediction and predictive control of systems governed by the nonlinear parabolic PDEs that describe continuous casting. Recent advances have been achieved in three such areas.

8.1 Robust Model Reference Adaptive Control of Parabolic and Hyperbolic Systems with Spatially-varying Parameters:

This problem is solved in [19] for a class of DPS described by parabolic and hyperbolic PDEs with spatially-varying coefficients, removing a key obstacle in applicability of the PDE-based model reference adaptive control (MRAC) of DPS to such problems as control of continuous steel casting. This work [19] introduces the class of DPS to be considered, provides the main background definitions, and clearly brings out the robustness deficiency problem with the existing MRAC laws for these DPS. This reference introduces a novel direct MRAC structure given below that eliminates the problem both for the parabolic and the hyperbolic cases (**Fig. 30**).

Plant: $u_t = (a(x)u_x)_x + b(x)u + f(x,t)$

Reference Model: $v_t = (a_1(x)v_x)_x + b_1(x)v + r(x,t)$

Adaptive control law: $f = r + \varepsilon_0 e + \eta_{a1} v_{xx} + \eta_{a2} v_x + \eta_b v$

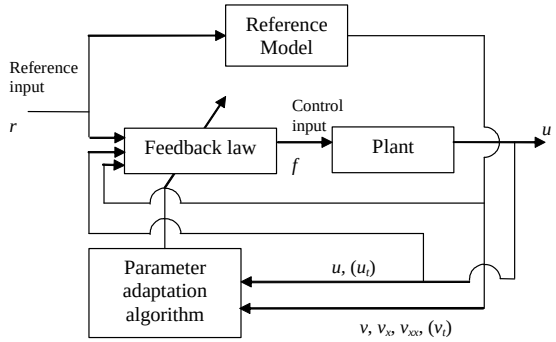

Fig. 30 Direct MRAC structure based control

The performance of this control law is shown in the following figure, **Fig. 31**.

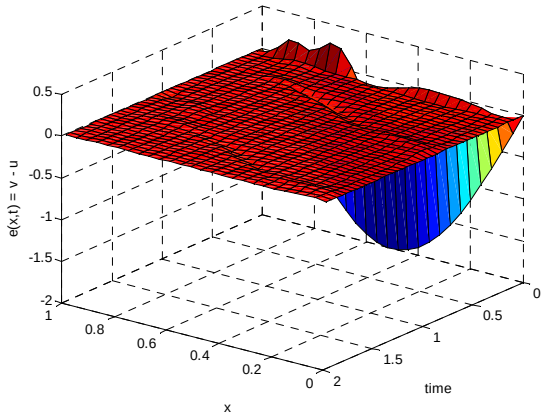

Fig. 31 Spatial and Temporal Variation of Error for Direct MRAC control law

In an effort to further enhance the performance and reduce the computational complexity of the control laws proposed when system parameters are characterized by a significant, not necessarily, smooth spatial variation, a technique for the finite-dimensionalization of the parameter adaptation laws based on multiresolution analysis is developed, as reported elsewhere. [20] For this purpose, a new tool - the multiresolution Lyapunov functional is introduced. Through the wavelet-based parameter decomposition, the technique is applied to parameter adaptation laws for both parabolic and hyperbolic PDEs. The laws are shown to admit a low order high fidelity finite-dimensionalization when the wavelet basis is matched to the main plant parameter features, such as nonsmoothness, known a priori. Using the corresponding multiresolution Lyapunov functional, the stability of the closed loop system with the finite-dimensional parameter adaptation law and the infinite-dimensional plant is rigorously proven for both equation types. The advantages of the finite-dimensionalization approach proposed - reduction of computational demand and increase in the output convergence rate with no corresponding increase in the control effort are demonstrated, as well. This work[20] develops finite-dimensionalization technique for the parameter adaptation laws proposed. Numerical simulations supporting the assertions made and showing attainment of good performance for the settings earlier characterized by instability are presented below.

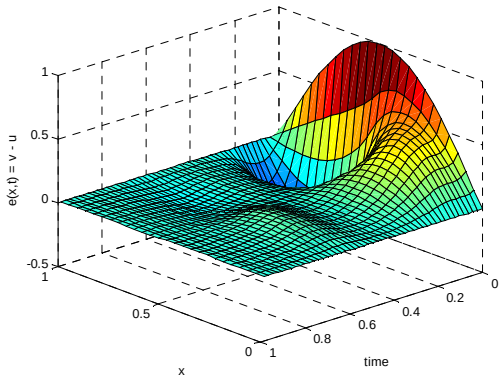

Fig. 32 Performance of infinite-dimensional technique

8.2 Disturbance Rejection in Robust Model Reference Adaptive Control of Parabolic and Hyperbolic Systems with Spatially-varying Parameters

This setting is of interest in a solidifying shell temperature control in continuous steel casting, where a single two-dimensional boundary control problem of the outer shell surface temperature shown in **Fig. 1** can be well approximated by a pair of one-dimensional distributed control problems of the outer shell surface temperature for the inner and the outer caster radii. This is accomplished by bringing in, as shown in the **Fig. 33** below, the near-constant distributed disturbance.

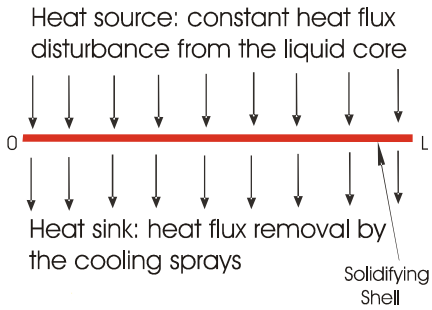

Fig. 33. Approximation of the single 2D shell surface temperature boundary control problem by the two - outer and inner radii - 1D shell surface temperature distributed control problems through the introduction of the constant distributed heat flux disturbance. The latter is induced at the liquid/solid interface by the molten steel core encased by the solidifying shell

The latter is characterized by an approximately known model and represents the heat flux at the interface between the inner surface of the solidifying shell and the liquid core. The disturbance is seen to lie in the system input space. Thinking along the lines of this approximation governs, to a large extent, current spray cooling control practice at some key steel casting facilities.

In this application, actuation is designed to be a very close approximation of the distributed one to ensure smooth cooling along the strand - the feature especially important in continuous thin slab metal casting due to the thinness of the solidifying shell, and a matching pyrometer array temperature sensing is being currently developed. The parameters of the casting process, such as heat transfer coefficients, are known to be periodic-like functions of a spatial variable due to the fact that the outer shell surface alternates between being in contact with the fixed position support rollers and being subject to the water flux from the sprays along the cooling zone of a caster. This functional dependence is known, however, only approximately, is influenced by a number of factors, such as steel grade and casting speed, and undergoes a slow time-variation caused by the solidifying shell motion. Reduction of uncertainty in this dependence is currently underway; however it proves to be very costly, time consuming, and requiring

nontrivial instrumentation. In addition, the pyrometer readings are characterized by a noticeable steam-induced spatiotemporal noise. \

This problem is solved in [21, 22]. Based on the well-posed MRAC configurations recently introduced [19, 20]that are free from plant output spatial derivatives, this work develops the well-posed error systems and the corresponding robust MRAC laws with disturbance rejection for a class of systems represented by parabolic or hyperbolic PDEs with spatially varying parameters. Disturbances are assumed to be generated by a known model and lie in the system input space. Control signal is, then, shown to include the disturbance estimate generated by the corresponding distributed parameter Luenberger-type observer. The well-posed error systems and the corresponding algorithms for parabolic and hyperbolic PDEs are derived, with the disturbance rejection properties exhibited in numerical simulations. For simplicity, derivations are carried out for a single spatial domain. The work considers distributed sensing and actuation as well as distributed disturbance. This setting is of interest in a number of applications, such as continuous steel casting.

Plant: $u_t = (a(x)u_x)_x + b(x)u + f(x,t) + d(x,t)$

Reference Model: $v_t = (a_1(x)v_x)_x + b_1(x)v + r(x,t)$

Adaptive control law: $f = r + \varepsilon_0 e + \eta_{a1} v_{xx} + \eta_{a2} v_x + \eta_b v$

Disturbance model: $d_t = (a_d(x)d_x)_x + f_d$

Schematics of adaptive controller and disturbance observer is given by **Fig. 34**.

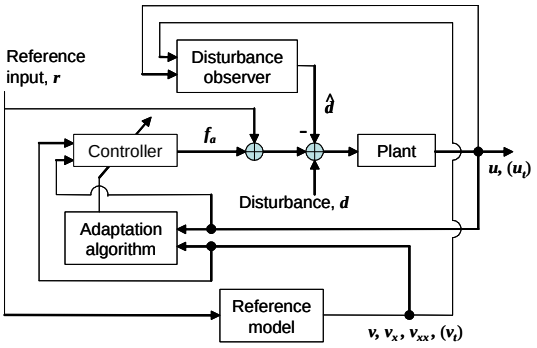

Fig. 34. Adaptive controller and disturbance observer

8.3. Bumpless Transfer: Smooth Online Switching Between the Currently Used Controller and the New Controller:

New algorithms for bumpless transfer have been developed to tackle the complex computational/communication environment, like the one at Nucor, where the analytical controller models cannot take into account time-varying computational/communication delays and other uncertainties. In this case, bumpless transfer based on the analytical controller model becomes unreliable. This problem is solved in [21] that establish a modern steady state bumpless transfer design paradigm - a hierarchy of optimal design techniques defined by the characteristics of controller uncertainty. Within this paradigm, the internal model based robust H_∞-optimal full information steady-state bumpless transfer synthesis handles the most general controller uncertainty; simplification of controller uncertainty structure reduces the latter technique to LQ state/output transfer, while complete elimination of uncertainty provides further reduction to Turner and Walker's LQ state transfer topology shown in **Fig. 35**. For the latter topology, a hybrid explicit controller switching operation is derived by the PIs. The paradigm is completed by indicating that all of the above techniques admit hybrid implementation, i.e. almost instantaneous controller transfer attained under controller uncertainty through computational speedup.

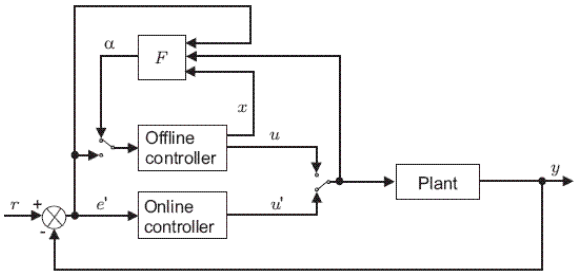

Fig. 35. The one-degree-of-freedom LQ bumpless transfer topology that is ameanable to instantaneous controller transfer.

Summary of Significant Findings:

A new online computer model-based control system is being created to control solidification and temperature development during the continuous casting of steel. It features an accurate and fundamentally-based dynamic software sensor of the spray-cooling region which is integrated with online measurements of mold heat extraction and other process parameters. By maintaining the steel temperature through operational transients, this system aims to enable faster and more efficient casting with improved quality of the steel product. This multi-faceted research project includes the development, validation, and calibration of the online control models, laboratory measurements to better characterize heat transfer during spray cooling, improved control algorithms, and increased understanding of defect formation in the continuous casting process. Work this past year has obtained several new findings, which are significant to the project goals. Most significant are:

- A novel modeling algorithm is able to update in real time, the complete solidification and temperature profile in two dimensions at every second during continuous online operation.

- The new control system maintains temperature more closely than the conventional control system currently in use at most plants.

- This new modeling tool is now available to study thin-slab casting behavior, to enable future process and control improvements.

- Better understanding of the control of defects arising during continuous casting has been achieved, including the control of fluid flow in the mold using electromagnetic braking, and cracks associated with the control of secondary cooling.

- New optimal control algorithms have been developed, with application to the systems and equations governing heat transfer in continuous casting.

Future improvements to this novel model-based control system should revolutionize the control of continuous casting spray systems, with improved steel quality, and will have beneficial impact on related scientific fields and commercial processes.

This report has summarized the results of eight different sub-projects which comprise this multi-faceted research project. Further details can be found in 21 publications[5, 9, 10, 12, 13, 17-32], a nonprovisional patent application,[8], and in the website http://ccc.mechse.uiuc.edu.

References:

1. Meng, Y. and B.G. Thomas, "Heat Transfer and Solidification Model of Continuous Slab Casting: CON1D," Metal. & Material Trans., Vol. 34B (5), 2003, 685-705.

2. Meng, Y. and B.G. Thomas, "Modeling Transient Slag Layer Phenomena in the Shell/Mold Gap in Continuous Casting of Steel," Metall. Mater. Trans. B, Vol. 34B (5), 2003, 707-725.
3. Santillana, B., L.C. Hibbeler, B.G. Thomas, A. Hamoen, A. Kamperman, W. van der Knoop, "Investigating Heat Transfer In Funnel-Mould Casting With CON1D: Effect of Plate Thickness," ISIJ Internat., Vol. 48 (10), 2008, 1380-1388.
4. Park, J.-K., B.G. Thomas, I.V. Samarasekera and U.-S. Yoon, "Thermal and Mechanical Behavior of Copper Moulds During Thin Slab Casting (I): Plant Trial and Mathematical Modelling," Metall. Mater. Trans., Vol. 33B (June), 2002, 425-436.
5. Thomas, B.G., J. Bentsman, B. Petrus, S. Vapalahti, H. Li, A.H. Castillejos and F.A. Acosta, "GOALI: Online Dynamic Control of Cooling in Continuous Casting of Thin Steel Slabs," in Proceedings of 2008 NSF CMMI Engineering Research and Innovation Conference, (Knoxville, Tennessee, Jan. 7-10, 2008), 2008, 16p.
6. Thomas, B.G. and C. Ojeda, "Ideal Taper Prediction for Slab Casting," ISSTech Steelmaking Conference, (Indianapolis, IN, USA, April 27-30, 2003), Vol. 86, 2003, 396-308.
7. Cicutti, C., MartinValdez, T. Perez, G. DiGresia, W. Balante and J. Petroni. Mould Thermal Evaluation in a Slab Continuous Casting Machine. Steelmaking Conference Proceedings. Vol. 85 (2002), 97-107.
8. B.G. Thomas, J. Bentsman and K. Zheng, "Cooling Control System for Continuous Casting of Metal," (U.S Nonprovisional Patent Application # TF07019), 2008.
9. Zheng, K., B. Petrus, B.G. Thomas and J. Bentsman, "Design and Implementation of a Real-time Spray Cooling Control System for Continuous Casting of Thin Steel Slabs,," in AISTech 2007, Steelmaking Conference Proceedings, Indianapolis, May 7-10, 2007, Association for Iron and Steel Technology, Warrendale, PA, USA, 2007.
10. Bryan Petrus, Kai Zheng, Xiaoxu Zhou, Brian G. Thomas and J. Bentsman, "Real-Time Model-Based Spray-Cooling Control System for Steel Continuous Casting," Metals and Materials Transactions B, 2009, submitted March, 2009; Revised July, 2009.
11. C. Edwards and I. Postlethwaitex, "Anti-windup and Bumpless Transfer Schemes," UKACC International Conference on CONTROL), 1996, 394-399.
12. Vapalahti, S., B. G. Thomas, S. Louhenkilpi, A.H. Castillejos, F. A. Acosta and C.A. Hernandez, "Heat Transfer Modelling of Continuous Casting: Numerical Considerations, Laboratory Measurements and Plant Validation," STEELSIM 2007, (Graz, Austria, Sept. 12-14, 2007), 2007.
13. Thomas, B.G., J. Bentsman, K. Zheng, S. Vapalahti, B. Petrus, A. Behera, A.H. Castillejos and F.A. Acosta, "Online Dynamic Control of Cooling in Continuous Casting of Thin Steel Slabs," in Proceedings of 2006 NSF Design, Service, and Manufacturing Grantees and Research Conference, W. DeVries and M. Leu, eds., (St. Louis, Missouri, July 24-27, 2006), 2006, 11p.
14. Meng, Y. and B.G. Thomas, "Simulation of Microstructure and Behavior of Interfacial Mold Slag Layers in Continuous Casting of Steel," ISIJ International, Vol. 46 (5), 2006, 660-669.
15. Sengupta, J., B.G. Thomas, H.J. Shin, G.G. Lee and S.H. Kim, "Mechanism of Hook Formation during Continuous Casting of Ultra-low Carbon Steel Slabs," Metallurgical and Materials Transactions A, Vol. 37A (5), 2006, 1597-1611.
16. Thomas, B.G., J.K. Brimacombe and I.V. Samarasekara, "The Formation of Panel Cracks in Steel Ingots : A State-of-the-Art Review : I. Hot ductility of Steel ; II. Mid-face and Off-corner cracks.," ISS Trans., Vol. 7, 1986, 7-29.
17. Kun Xu and B.G. Thomas, "Prediction of Grain Size, Precipitation, and Crack Susceptibility in Continuous Casting," AISTech 2009 Steelmaking Conference Proc., (St. Louis, MO, May 4-7, 2009), Assoc. Iron Steel Tech., Warrendale, PA, Vol. 1, 2009.
18. Cukierski, K. and B.G. Thomas, "Flow Control with Local Electromagnetic Braking in Continuous Casting of Steel Slabs," Metallurgical and Materials Transactions B, Vol. 39B (1), 2008, 94-107.
19. Kim, J. and J. Bentsman, "Robust Model Reference Adaptive Control of Parabolic and Hyperbolic Systems with Spatially-varying Parameters," 44th IEEE Conference on Decision and Control, (Seville, Spain, Dec. 13-15, 2005), 2005, 1503-1508.
20. Kim, J. and J. Bentsman, "Multiresolution Finite-Dimensionalization of Parameter Update Laws in Adaptive Control of Distributed Parameter Systems," 45th IEEE Conference on Decision and Control, (San Diego, CA, Dec. 13-15, 2006), 2006, 2801-2806.
21. Kim, J. and J. Bentsman, "Disturbance Rejection in Robust Model Reference Adaptive Control of Parabolic and Hyperbolic Systems," 45th IEEE Conference on Decision and Control, (San Diego, CA, Dec. 13-15, 2006), 2006, 3083-3088.

22. Kim, J. and J. Bentsman, "Disturbance Rejection in a Class of Adaptive Control Laws for Distributed Parameter Systems," International Journal of Adaptive Control and Signal Processing, Vol. 23, 2009, 166-192.
23. Thomas, B.G. and K. Cukierski, "Flow Control with Local Electromagnetic Braking in Continuous Casting of Steel Slabs," in Third Baosteel Biennial Conference, Vol. 1, (Shanghai, PRC (September 25-26, 2008)), 2008, 94-107.
24. Zheng, K., J. Bentsman and C.W. Taft, "Bumpless Transfer under Controller Uncertainty: Theory and Implementation," in Proceeding of the 45th IEEE Conference on Decision and Control, (San Diego, CA, 6247-6252, Dec. 12-15, 2006), 2006.
25. Zheng, K., T. Başar and J. Bentsman, "H∞ Bumpless Transfer under Controller Uncertainty," IEEE Transactions on Automatic Control, Vol. 54, 2009, 1718-1723.
26. Zheng, K. and J. Bentsman, "Decentralized Compensation of Controller Uncertainty in the Steady-State Bumpless Transfer Under the State/Output Feedback," International Journal of Robust and Nonlinear Control, 2009, in press.
27. Zheng, K. and J. Bentsman, "Input/Output Structure of the Infinite Horizon LQ Bumpless Transfer and Its Implications for Transfer Operator Synthesis," International Journal of Robust and Nonlinear Control, 2009, in press.
28. Zheng, K., T. Başar and J. Bentsman, "H∞ Bumpless Transfer under Controller Uncertainty," in Proceeding of the 46th IEEE Conference on Decision and Control, (New Orleans, LA, Dec. 12-14, 2007), 2007, 2129-2134.
29. Vapalahti, S., H. Castillejos, Andrés Acosta, Alberto C. Hernández and B.G. Thomas, "Spray Heat Transfer Research at CINVESTAV," University of Illinois, June 12, 2007, Continuous Casting Consortium Report CCC0704, 2007.
30. Vapalahti, S., H. Castillejos, Andrés Acosta, Alberto C. Hernández and B.G. Thomas, "Delavan Nozzle Characterization Research at CINVESTAV," University of Illinois, June 12, 2007, Continuous Casting Consortium Report CCC0703, 2007.
31. Thomas, B.G., "Industry Implementaion of Mathematical Models: Examples in Steel Processing, Howe Memorial Lecture," in AISTech Steelmaking Conference Proceedings, Vol. 1, Assoc. Iron Steel Tech., Warrendale, PA, (St. Louis, MO, May 4-7, 2009), 2009.
32. Thomas, B.G., J. Bentsman, B. Petrus, H. Li, A.H. Castillejos and F.A. Acosta, "GOALI: Online Dynamic Control of Cooling in Continuous Casting of Thin Steel Slabs," in Proceedings of 2009 NSF CMMI Engineering Research and Innovation Conference, National Science Foundation, (Honolulu, Hawaii, June 22-25, 2009.), 2009, 16p.